Electronic Supplementary Material (ESI) for ChemComm.
This journal is © The Royal Society of Chemistry 2023

Electronic Supplementary Information

Ammonium fluoride additives modified interphase chemistry stabilizes zinc anodes in aqueous electrolytes

*Wei Zhang, ‡[ab] Xian Wu, ‡[b] Qingjin Fu, ‡[b] Haotian Qu, [b] Joanna Borowiec, [a] Mark Isaacs, [a] Guangmin Zhou, [b] Ivan P. Parkin, *[a] and Guanjie He*[a]*

[a] *Christopher Ingold Laboratory, Department of Chemistry, University College London, London WC1H 0AJ, UK. E-mail: i.p.parkin@ucl.ac.uk; g.he@ucl.ac.uk*

[b] *Tsinghua Shenzhen International Graduate School, Tsinghua University, Shenzhen 518055, P. R. China.*

Electrolyte and electrode preparation

0.25 mol $ZnSO_4 \cdot 7H_2O$ (> 99%, VWR chemicals) were initially dissolved into 250 mL deionized water to prepare 1 M $ZnSO_4$ electrolyte (BE). Proper amounts of NH_4F (NF; ≥ 98.0%, Sigma-Aldrich) powders were then added into 5 mL as-prepared 1 M $ZnSO_4$ solution to keep the concentrations of the additives as 10 mM, 25 mM, and 50 mM. The optimized one is 25 mM NF (DE). 70% (gravimetric ratio) commercial MnO_2 (precipitated active for synthesis, Sigma-Aldrich) were mixed up with 10% poly(vinylidene fluoride) (average M_w ~534000, Sigma-Aldrich) and 20% acetylene black (battery grade, MTI) in N-methyl-2-pyrrolidine (≥ 99%, Sigma-Aldrich) solvent to prepared the cathode slurry, which was subsequently dried in a 60 ^oC vacuum oven for 24 h. Hydrophilic carbon paper (TORAY) served as the current collector.

Characterizations

A JEOL-JSM-6700F device (voltage: 5 kV, emission current: 110.8 μA) was carried out to observe the micro-morphologies under a low vacuum of $< 3\times10^{-4}$ Pa. The *in-situ* optical microscope was performed on a VisiScope® BL254 T1 (VWR) device with a Zn||Zn symmetric configuration. XRD patterns of zinc foils were collected on a PANalytical Empyrean instrument (radiation: Cu-K_α). The XRD pattern of the commercial MnO_2 powder was collected on a STOE SEIFERT diffractometer (radiation: Mo-K_α). AZ9861 pH meter (AZ Instrument Corp.) was taken to measure the pH values. Raman spectra were obtained from Bruker Senterra Raman Specrometer (laser wavelength: 532 nm). Bruker Vertex 70 spectrophotometer was taken to collect the FT-

IR results after deducting the background signal. Thermo Scientific spectrometer was taken to collect the XPS data with a monochromatic Al-K_α source. XPS spectra were calibrated by the C 1s of 284.8 eV. The binding energies were referred to the National Institute of Standards and Technology (NIST, USA) database.

Electrochemical measurements

Zinc-based batteries were assembled in the CR2032 coin cell with glass fiber separator (Whatman GF/A). The amounts of electrolyte for each coin cell were controlled as 80 μL. Zinc foils (ϕ12 mm circles; 20 μm in thickness) were used in Zn||Zn symmetric cells, Zn||Cu asymmetric cells, and Zn||MnO_2 full cells. All electrochemical performances were measured in the Neware battery test system (CT-4008T-5V50mA-164, Shenzhen, China). 0.1 M $MnSO_4$ was further added to suppress the Mn dissolution for Zn||MnO_2 full cells, which were pre-cycled for 10 cycles at 0.2 A g^{-1} prior to cyclic and rate performances measurements. A Biologic VMP-3 electrochemical workstation was taken to conduct chronoamperometry (CA) of Zn||Zn cells at -150 mV, linear polarization curves at 1 mV s^{-1} and LSV curves at 10 mV s^{-1} with Ag/AgCl as the reference electrode.

DFT calculation details

All theoretical works were conducted by using the projector augmented wave approach in the framework of the density functional theory (DFT),[1] as performed in the QUANTUM ESPRESSO.[2] The generalized gradient approximation (GGA) and Perdew–Burke–Ernzerhof (PBE) exchange functional[1] was carried out. The plane-

wave energy cutoff was set to 38 Ry, and the Monkhorst–Pack method[3] is employed for the Brillouin zone sampling. The convergence criteria of energy and force calculations were set to 10^{-5} Ry/atom and 0.01 Ry/Å, respectively. The Zn surface model was built by the 2×6 supercell of Zn (101). A vacuum region of 15 Å is applied to avoid interactions between the neighboring configurations. DFT-D2 method was used to account for the vdW interactions between Zn (101) surface and molecule (ion).[4] To explore the interactions between the molecule (ion) and Zn surface, the adsorption energies of the molecule (ion) adsorption on Zn (101) surface were calculated. Here, the adsorption energies (E_{ad}) were calculated by the energy difference of the system after and before adsorption:[5] E_{ad}= E(Ion adsorbed Zn) - E(Ion) - E(Zn), where E(Ion adsorbed Zn), E(Ion) and E(Zn), represent the DFT energies of the ion or molecule adsorbed Zn surface, the energy of an ion or molecule, and the energy of clean Zn surface, respectively.

Finite element modelling

The Zinc deposition simulation was performed with the COMSOL Multiphysics 6.1. Tertiary current distribution module and deformed geometry module were used to study the electrolyte current density distribution and negative electrode deposition, further, the results of the Zinc deposition and electrochemical simulation can be simultaneously determined by the Multiphysics coupling interface “Deform the electrode surface”.

In the electrolyte, the Zn-ion transport driven by the concentration gradient and electromigration was governed by the Nernst–Planck equation:

$$N_{\mathbf{Zn+}} = -D_{\mathbf{Zn+}} + \left(\nabla c_{\mathbf{0}} - \frac{zFc_0}{RT}\nabla\Phi\right)$$

where the N_{Zn+} is Zn-ion flux, D_{Zn+} is the diffusion coefficient of Zn-ion in the electrolyte, z is the charge of Zn-ion, c_0 is the concentration of Zn-ion in the electrolyte, F is the Faraday's constant, R is the ideal gas constant, T is the Kelvin temperature, and Φ is the electrolyte potential.

Meanwhile, zinc ions in electrolyte follow the mass and charge conservation equations:

$$\frac{\partial c_{Zn^{2+}}}{\partial t} + \nabla \times N_{Zn^{2+}} = 0$$

$$\sum_i z_i c_i = 0$$

At the interface of the electrolyte and the anode, the deposition reaction of zinc ions can be described by the reaction below:

$$Zn^{2+} + 2e^- \rightleftharpoons Zn$$

The deposition behavior of zinc ions near substrate is determined by the local current density, which is governed by the Butter-Volmer equation:

$$N_{\mathbf{Zn+}}n = -\frac{i_0}{2F}\left[\exp\left(\frac{\alpha_a F\eta}{RT}\right) - \frac{c_{\mathbf{Zn+}}}{c_0}\exp\left(\frac{\alpha_a F\eta}{RT}\right)\right]$$

where i_0 is exchange current density, η is overpotential, α_a and α_c are the anodic and cathodic charge transfer coefficients, respectively, and $c_{\mathbf{Zn+}}$ is the concentration of Zn-ion near the interface.

Furthermore, in deformed geometry module, the morphology of Zn-ion deposition could be simulated through the normal velocity near the anode which was calculated from the local current density, and the normal velocity was defined as:

$$v_n = \frac{-2FN_{\mathbf{Zn+}}n}{nF}\frac{M}{\rho}$$

where M and ρ are the molar mass and density of zinc.

Thus, the morphology of zinc dendrites is determined by the velocity in the normal direction near the surface:

$$v_n = n \cdot \frac{dy}{dt}$$

The geometry area was 100 μm × 50 μm. Both of the anodic and cathodic charge transfer coefficients were set as 0.5, the temperature was fixed at room temperature and the applied current density was set as 1 mA cm^{-2} The time of zinc ions deposition was set as 3 hours to observe the evolution of anode morphology. By regulating the speed of mass transport for zinc ions, different deposition morphology can be obtained.

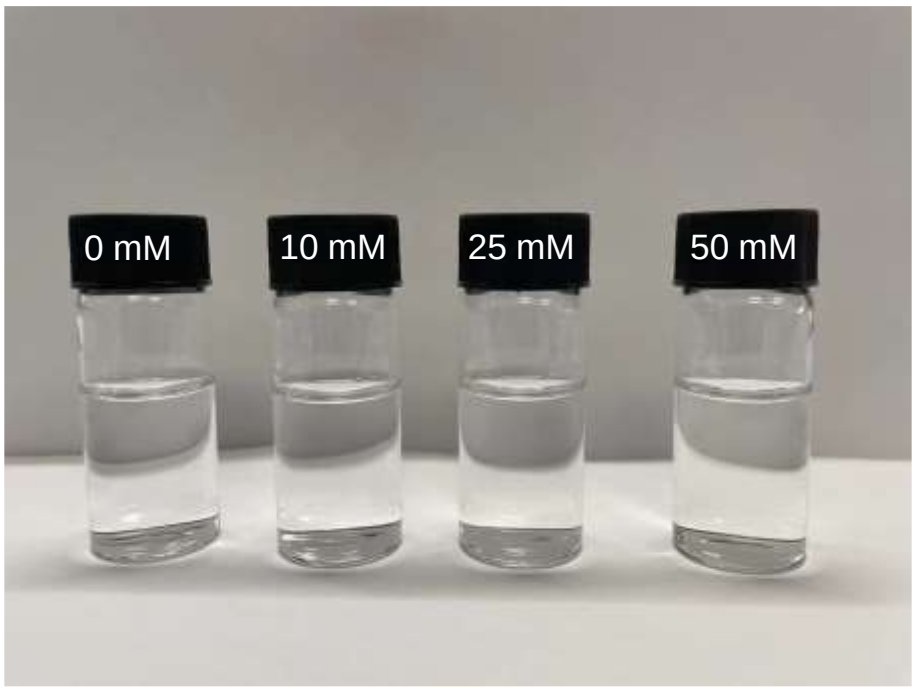

Fig. S1 Digital photographs of the NF containing electrolytes.

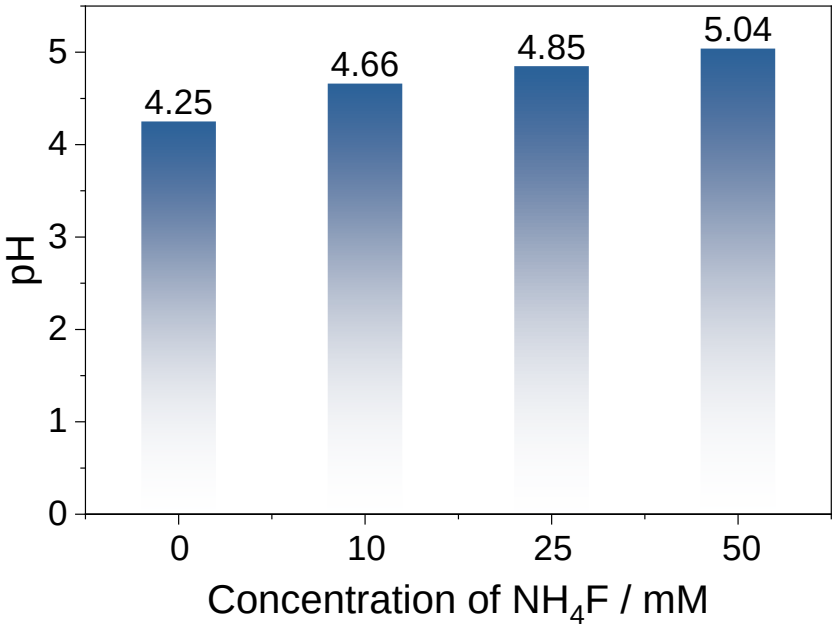

Fig. S2 pH values of the NF containing electrolytes.

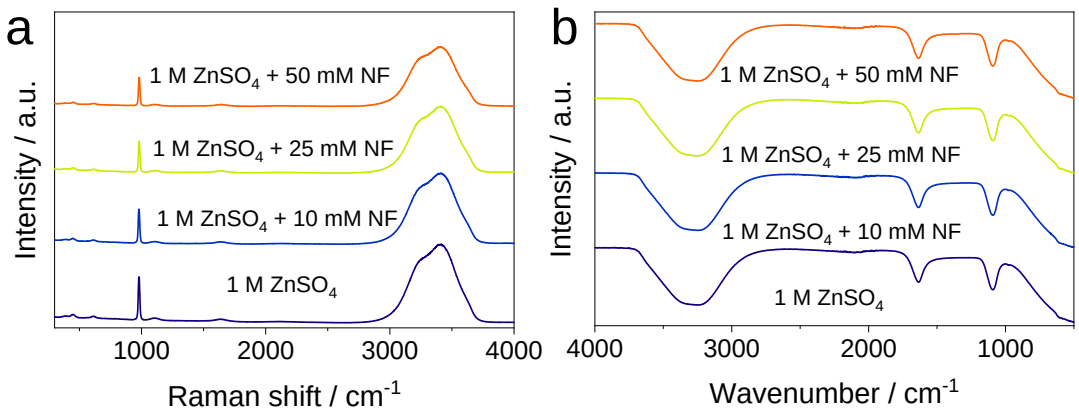

Fig. S3 (a) FT-IR spectra and (b) Raman spectra of different electrolytes.

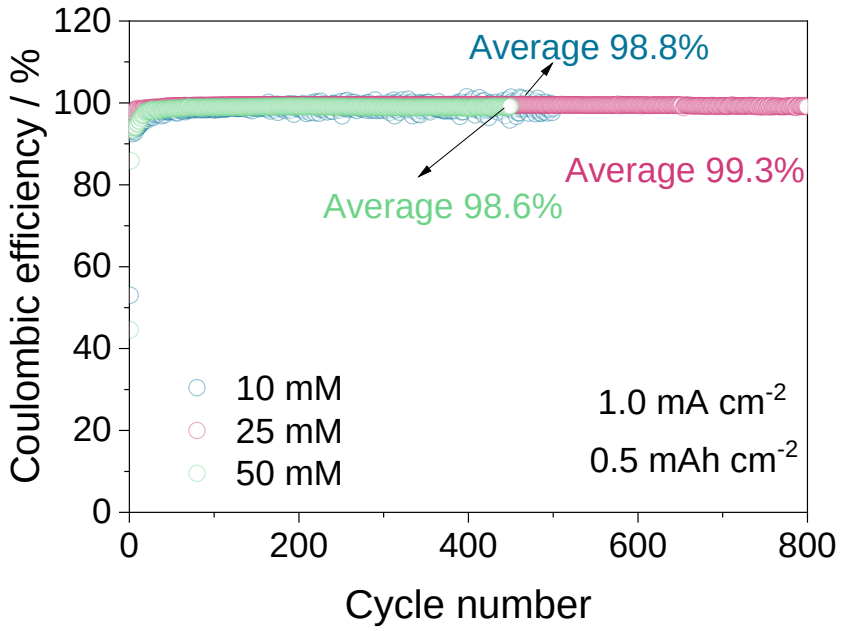

Fig. S4 Coulombic efficiencies of Zn||Cu cells on a "anode-free" mode[6] with different NF containing electrolytes at 1 mA cm^{-2} with a fixed capacity of 0.5 mAh cm^{-2}.

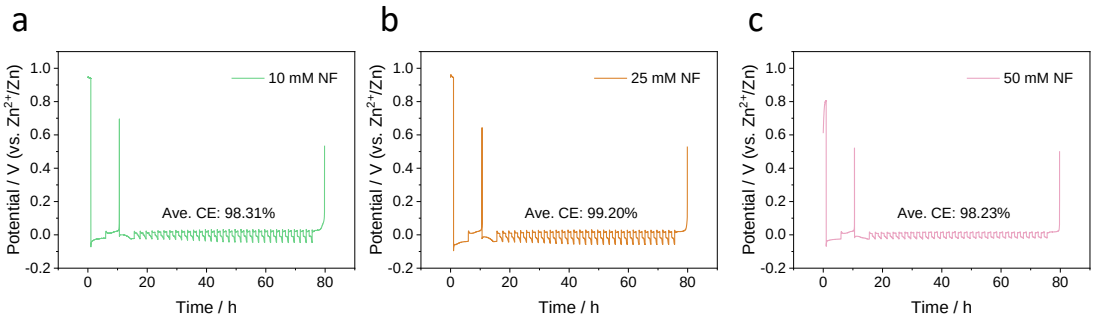

Fig. S5 Coulombic efficiencies of Zn||Cu cells on a hybrid mode[6] (the 1st cycle: discharging/charging for 5 h at 1 mA cm^{-2}; subsequent cycles: discharging/charging for 1 h for each cycle; cut-off voltage for the last charging process was 0.5 V (vs. Zn^{2+}/Zn)) with different NF containing electrolytes.

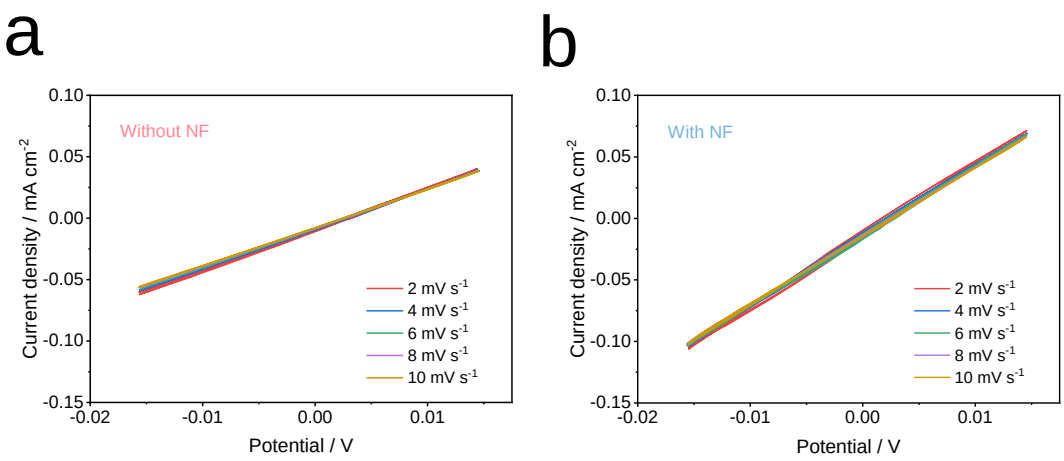

Fig. S6 Cyclic voltammograms curves for Zn || Zn symmetric coin cells in a voltage range of –15 mV to 15 mV under various scanning rates in (a) BE and (b) DE.

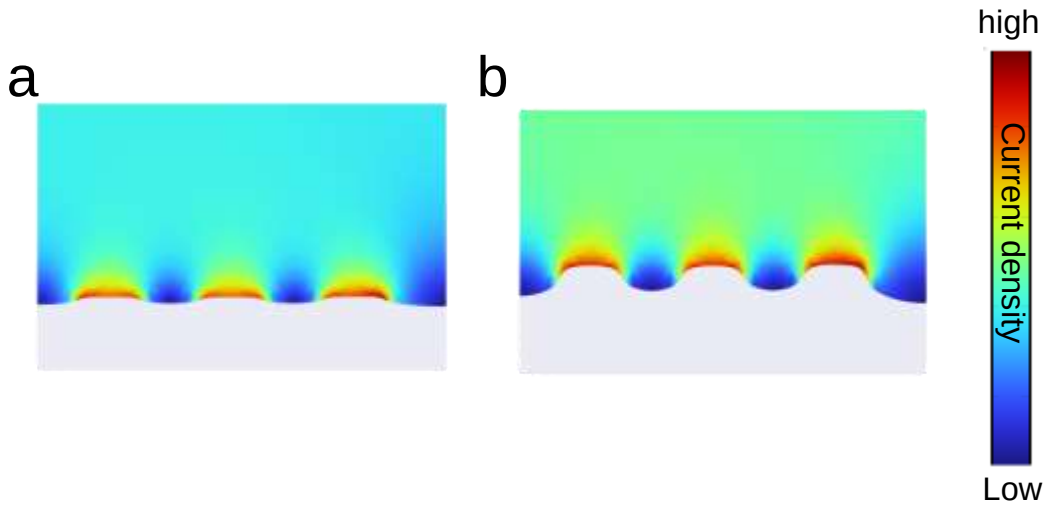

Fig. S7 COMSOL simulations of current density of Zn anodes in (a) DE and (b) BE.

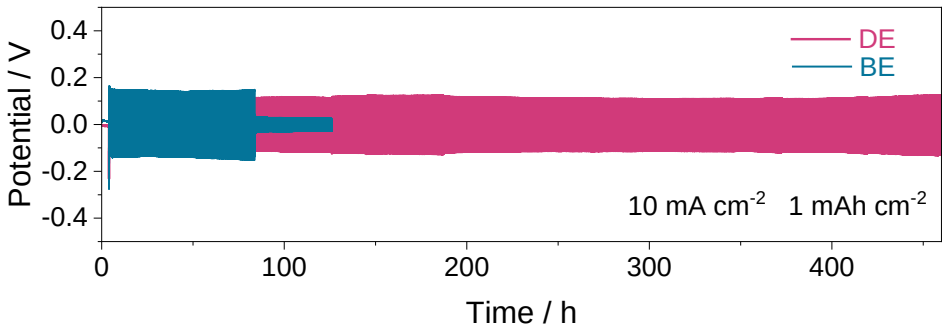

Fig. S8 Plating/stripping cyclabilities of Zn||Zn symmetric cells under 1 M $ZnSO_4$ (BE) and 1 M $ZnSO_4$ + 25 mM NF (DE) at 10 mA cm^{-2} with a capacity of 1 mAh cm^{-2}.

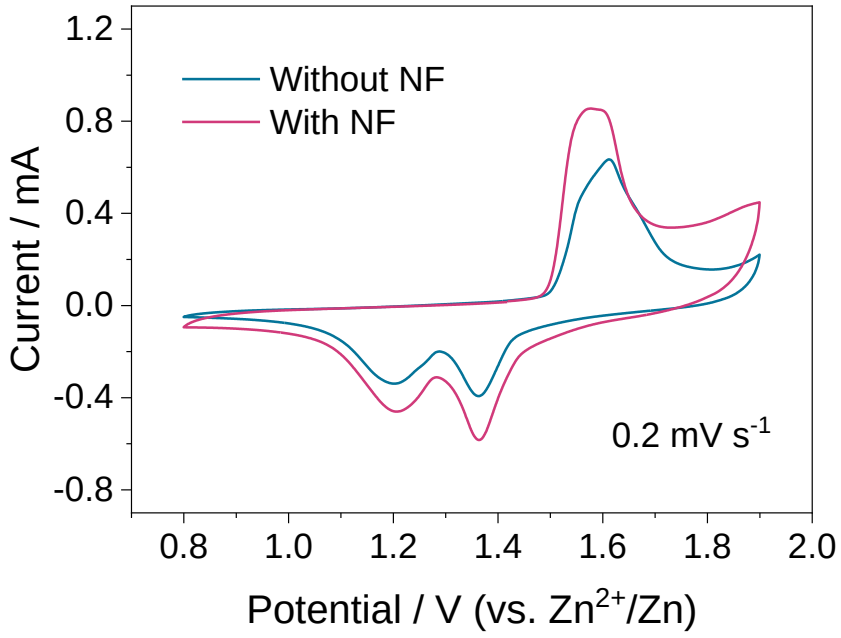

Fig. S9 CV curves of Zn||MnO_2 cells with or without NF additives.

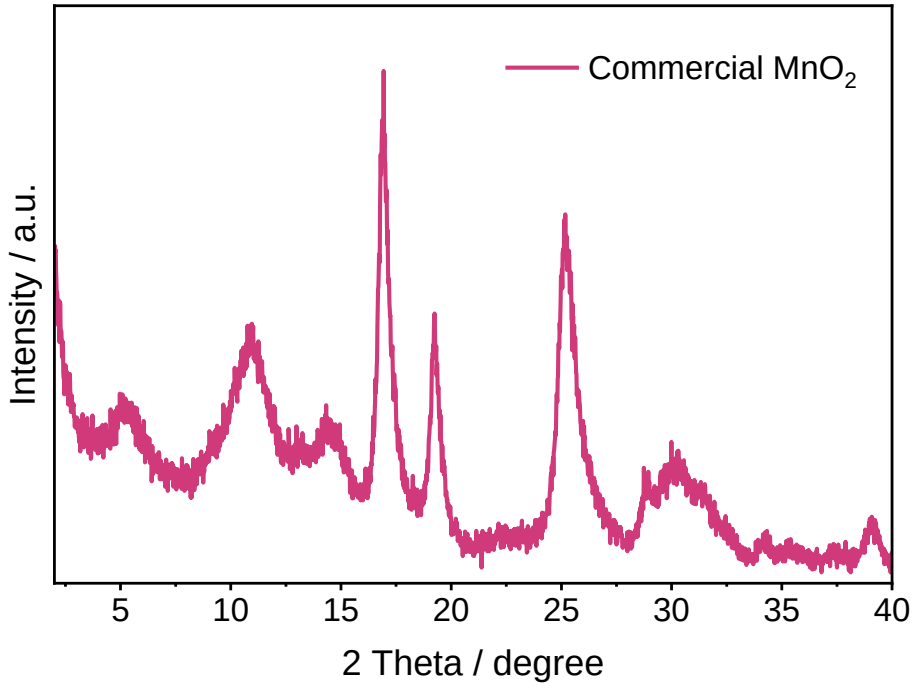

Fig. S10 XRD pattern of the commercial MnO_2 powder under the Mo-K_α radiation.

Table S1. The comparison of this work with other previous aqueous electrolytes for zinc metal anodes.

Electrolyte (M: mol L^{-1}; m: mol kg^{-1})	Symmetric Zn cells		Asymmetric Zn cells			Ref.
	Current Density (mA cm^{-2})/ Capacity (mAh cm^{-2})	Lifespan (hours)	Current Density (mA cm^{-2})/ Capacity (mAh cm^{-2})	Average CE	Lifespan (cycles)	
1 M $ZnSO_4$+ 25 mM NH_4F	1/1 4/0.5	1450 1100	1/0.5	99.3%	800	This work
30 m $ZnCl_2$	0.2/0.033	600	1/0.4	95.4%	95	7
2 M $ZnSO_4$+0.05 mM TBA_2SO_4	2/2 5/5	300 160	10/10	98%	1	8
1.3 m $ZnCl_2$/H_2O-DMSO (H_2O/DMSO = 4.3:1 by volume)	0.5/0.5	1000	1/0.5	99.5%	400	9
3 m $ZnSO_4$+2 m LiCl	1/1	125	N.A.	N.A.	N.A.	10
2 M $ZnSO_4$+0.1 M BIS-TRIS	1/1	1200	1/1	98.5%	400	11
2 M $ZnSO_4$+0.05 mg mL^{-1} $Ti_3C_2T_x$ MXene	1/1 4/1	1000 250	1/1	98.32%	120	12
1 M $ZnSO_4$+10 mM glucose	2/2	700	1/0.5	97.2%	230	13
2 M $ZnSO_4$+0.5 g L^{-1} TMBAC	1/2	1000	1/1	99%	200	14
5 m $ZnCl_2$+5 m Betaine	0.5/0.5	1400	0.5/0.5	98%	400	15
1 M $Zn(ClO_4)_2$+10 mM β-cyclodextrin	1/1	1000	N.A.	97.6%	530	16
2 M $ZnSO_4$+ 10 mM Cysteine	0.5/0.5	2300	5/5	99.4%	280	17
2 M $ZnSO_4$+ 10 vol.% DMA	1/5	250	2/1	98.7	250	18

*Note: Tetrabutylammonium sulfate (TBA_2SO_4); Dimethyl sulfoxide (DMSO); 2Bis(2-hydroxyethyl) amino-2-(hydroxymethyl)-1,3-propanediol (BIS-TRIS); Benzyltrimethylammonium chloride (TMBAC); *N*,*N*-Dimethylacetamide (DMA)

Supplementary references

1 W. Kohn and L. J. Sham, *Phys. Rev.*, 1965, **140**, A1133-A1138.

2 P. Giannozzi, S. Baroni, N. Bonini, M. Calandra, R. Car, C. Cavazzoni, D. Ceresoli, G. L. Chiarotti, M. Cococcioni, I. Dabo, A. Dal Corso, S. de Gironcoli, S. Fabris, G. Fratesi, R. Gebauer, U. Gerstmann, C. Gougoussis, A. Kokalj, M. Lazzeri, L. Martin-Samos, N. Marzari, F. Mauri, R. Mazzarello, S. Paolini, A. Pasquarello, L. Paulatto, C. Sbraccia, S. Scandolo, G. Sclauzero, A. P. Seitsonen, A. Smogunov, P. Umari and R. M. Wentzcovitch, *J. Phys. Condens. Matter.*, 2009, **21**, 395502.

3 H. J. Monkhorst and J. D. Pack, *Phys. Rev. B*, 1976, **13**, 5188-5192.

4 S. A. Grimme, J.; Ehrlich, S.; Krieg, H. A, *J. Chem. Phys*, 2010, **132**, 154104.

5 Z. Xu, X. Lv, J. Chen, L. Jiang, Y. Lai and J. Li, *Carbon*, 2016, **107**, 885-894.

6 X. Yu, Z. Li, X. Wu, H. Zhang, Q. Zhao, H. Liang, H. Wang, D. Chao, F. Wang, Y. Qiao, H. Zhou and S.-G. Sun, *Joule*, 2023, **7**, 1145-1175.

7 C. Zhang, J. Holoubek, X. Wu, A. Daniyar, L. Zhu, C. Chen, D. P. Leonard, I. A. Rodriguez-Perez, J. X. Jiang, C. Fang and X. Ji, *Chem. Commun.*, 2018, **54**, 14097-14099.

8 A. Bayaguud, X. Luo, Y. Fu and C. Zhu, *ACS Energy Lett.*, 2020, **5**, 3012-3020.

9 L. Cao, D. Li, E. Hu, J. Xu, T. Deng, L. Ma, Y. Wang, X. Q. Yang and C. Wang, *J. Am. Chem. Soc.*, 2020, **142**, 21404-21409.

10 X. Guo, Z. Zhang, J. Li, N. Luo, G.-L. Chai, T. S. Miller, F. Lai, P. Shearing, D. J. L. Brett, D. Han, Z. Weng, G. He and I. P. Parkin, *ACS Energy Lett.*, 2021, **6**, 395-403.

11 M. Luo, C. Wang, H. Lu, Y. Lu, B. B. Xu, W. Sun, H. Pan, M. Yan and Y. Jiang, *Energy Storage Mater.*, 2021, **41**, 515-521.

12 C. Sun, C. Wu, X. Gu, C. Wang and Q. Wang, *Nano-Micro Lett.*, 2021, **13**, 89.

13 P. Sun, L. Ma, W. Zhou, M. Qiu, Z. Wang, D. Chao and W. Mai, *Angew. Chem. Int. Ed.*, 2021, **60**, 18247-18255.

14 K. Guan, L. Tao, R. Yang, H. Zhang, N. Wang, H. Wan, J. Cui, J. Zhang, H. Wang and H. Wang, *Adv. Energy Mater.*, 2022, **12**, 2103557.

15 Z. Jia, W. Zhao, S. Hu, X. Yang, T. He and X. Sun, *Chem. Commun.*, 2022, **58**, 8504-8507.

16 M. Qiu, P. Sun, Y. Wang, L. Ma, C. Zhi and W. Mai, *Angew. Chem. Int. Ed.*, 2022, **61**, e202210979.

17 Q. Meng, R. Zhao, P. Cao, Q. Bai, J. Tang, G. Liu, X. Zhou and J. Yang, *Chem. Eng. J.*, 2022, **447**, 137471.

18 F. Wu, Y. Chen, Y. Chen, R. Yin, Y. Feng, D. Zheng, X. Xu, W. Shi, W. Liu and X. Cao, *Small*, 2022, **18**, 2202363.